Taylor & Francis
Taylor & Francis Group

Estimating joint kinematics from skin motion observation: modelling and validation

Alon Wolf* and Merav Senesh

Biorobotics and Biomechanics Lab, Faculty of Mechanical Engineering, Technion – Israel Institute of Technology, Haifa 32000, Israel

Modelling of soft tissue motion is required in many areas, such as computer animation, surgical simulation, 3D motion analysis and gait analysis. In this paper, we will focus on the use of modelling of skin deformation during 3D motion analysis. The most frequently used method in 3D human motion analysis involves placing markers on the skin of the analysed segment which is composed of the rigid bone and the surrounding soft tissues. Skin and soft tissue deformations introduce a significant artefact which strongly influences the resulting bone position, orientation and joint kinematics. For this study, we used a statistical solid dynamics approach which is a combination of several previously reported tools: the point cluster technique (PCT) and a Kalman filter which was added to the PCT. The methods were tested and evaluated on controlled human-arm motions, using an optical motion capture system (Vicon^{TM}).

The addition of a Kalman filter to the PCT for rigid body motion estimation results in a smoother signal that better represents the joint motion. Calculations indicate less signal distortion than when using a digital low-pass filter. Furthermore, adding a Kalman filter to the PCT substantially reduces the dispersion of the maximal and minimal instantaneous frequencies. For controlled human movements, the result indicated that adding a Kalman filter to the PCT produced a more accurate signal. However, it could not be concluded that the proposed Kalman filter is better than a low-pass filter for estimation of the motion. We suggest that implementation of a Kalman filter with a better biomechanical motion model will be more likely to improve the results.

Keywords: rigid body motion estimation; soft tissue deformation; PCT; Kalman filter

1. Introduction

Typical joint movement during normal function involves a complex set of coupled translation and rotation. Consequently, motion analysis requires the estimation of 3D position and orientation of bones during movement. Stereo-photogrammetry is one of the commonly used measurement methods for 3D motion analysis. It allows for reconstruction of the trajectories of markers attached to the skin surface of the body segment that is being analysed. These trajectories are used to calculate the pose of the underlying bone, with the erroneous assumption that markers and bone segments are rigidly connected. It is well known that markers on the surface (i.e. skin) of the body move with respect to the underlying bones, and the motion is task dependent (Macleod and Morris 1987; Lafortune and Lake 1991; Fuller et al. 1997; Reinschmidt et al. 1997; Manal et al. 2003; Ryu et al. 2003; Leardini et al. 2005). It has also been observed that attempts to remove soft tissue artefacts through traditional filtering techniques can result in loss of information (Fuller et al. 1997; Cappello et al. 2005; Leardini et al. 2005). Consequently, soft tissue artefacts have been recognised as the major source of error in human motion analysis and are the primary factor limiting the resolution of detailed joint movements using skin-based systems.

The majority of studies describing 3D *in vivo* segment motions do not account for errors associated with non-rigid body movement, i.e. skin deformation. Several investigators have described methods designed to reduce errors associated with non-rigid segment movement (Che'ze et al. 1995; Cappello et al. 1997; Lu and O'Connor 1999; Alexander et al. 2003; Anand and Krishna 2004; Cerveri et al. 2004; Cappello et al. 2005). In general, these techniques model the limb segment as a rigid body and then apply various estimation algorithms to obtain an optimal estimate of the underlying skeletal motion, subject to a rigid body constraint (Goldstein 1980; Andriacchi et al. 1998). Other examples: the motion of the skin markers can be minimised by least square methods (Spoor and Veldpaus 1980; Veldpaus et al. 1988; Soderkvist and Wedin 1993; Challis 1995) or can be specifically modelled (Ball and Pierrynowski 1998; Alexander and Andriacchi 2001; Camomilla et al. 2009; Ryu et al. 2009). Observing all these studies, one can see that an exact modelling of the soft tissue deformation has not yet been developed, and perhaps never will be, due to its complex structure and nonlinear viscoelastic mechanical behaviour. A very comprehensive review, which provides an overview on quantification of soft tissue artefact in lower limb human motion analysis, was published recently. The authors concluded that more research is required in order to

---

*Corresponding author. Email: alonw@technion.ac.il

progress our understanding of soft tissue artefact and devise effective methods compensating for it in 3D human motion analysis (Peters et al. 2010).

We approached the problem of compensating for soft tissue artefacts by using a statistical solid dynamics method (Wolf and Mor 2008): a combination of several existing tools based on a least squares optimisation of the marker's position and orientation. We present the evaluation of this method on data collected during controlled human hand motion trials.

2. Methodology: a short summary

2.1 Point cluster technique (PCT)

The PCT (Andriacchi et al. 1998) is based on a cluster of points uniformly distributed on each segment. Each point is assigned an arbitrary scalar which can be varied at each time step and serves as a weighting factor in the optimisation. In this way, the contribution of a marker with a large noise to the transformation calculation can be factored down by assigning a low weight factor to the marker, and the transformation will be based mainly on markers that are less influenced by soft tissue deformation.

The inertia tensor eigenvalues form a basis for the optimisation technique, because they should remain invariant if the segment moves as a rigid body (Goldstein 1980). If non-rigid body movement occurs, the eigenvalues change during movement. An algorithm was developed (Andriacchi et al. 1998) to minimise the eigenvalue changes by redistributing the weight factors at each time step. At each time step, the eigenvalues and the sum of squares of the three eigenvalues (eigenvalues norm) are calculated as a function of the mass distribution:

$$\Lambda_i = \sqrt{(\lambda_i)_1^2 + (\lambda_i)_2^2 + (\lambda_i)_3^2}. \quad (1)$$

The difference between Λ_0 (eigenvalues norm at rest position) and Λ_s (eigenvalues norm at t_s) could be calculated in terms of n cluster point masses for each time step. This difference is defined as a function:

$$F = (\Lambda_s - \Lambda_0)^2. \quad (2)$$

Minimisation of F is then solved numerically using an unconstrained nonlinear optimisation operator in Matlab[TM]. The mass distribution is defined in terms of a single distribution parameter and calculated so that the point with the largest displacement from the rest position in the local (cluster) coordinate system is assigned the lowest weighting factor. For more details see (Wolf and Mor 2008).

2.2 Kalman approach to kinematic estimation

The Kalman filter is one of the most useful tools available today for estimating the state of a dynamic system in the presence of noise (Choset et al. 2005). For the Kalman filter to provide good results, the state function of each variable should represent the true dynamics as accurately as possible. In the case of no dynamic model of the motion, the state function can be formulated using numerical differentiation (Fioretti and Jetto 1989; Cerveri et al. 2003; Cerveri et al. 2004). A more detailed description of the use of the Kalman filter to improve data analysis of motion measurements can be found in Wolf and Mor (2008).

3. Motion analysis of a rigid body and a human forearm random motion

In this experiment, the position of markers attached to a rigid body and a human forearm (Figure 1) in a local coordinate system was calculated. The motions studied were random rotations of the rigid body and the forearm without any external constraints. Markers that were attached both to the rigid body and to the forearm were tracked using an eight-camera Vicon[TM] MX-13 system (Vicon Motion Systems and Peak Performance Inc. 2007).

3.1 Rigid body assumption

A rigid body assumption was taken, meaning a uniform mass-weighting factor was assigned to all cluster markers (Fioretti and Jetto 1989). However, for the markers attached to the forearm, bigger movements were expected because the markers were attached to the skin. The standard deviation of each point coordinate was calculated for both objects, i.e. rigid body and forearm, and the results are shown in Figures 2 and 3. Note that the point number shown in Figures 2 and 3 correlates to the markers numbered in Figure 1.
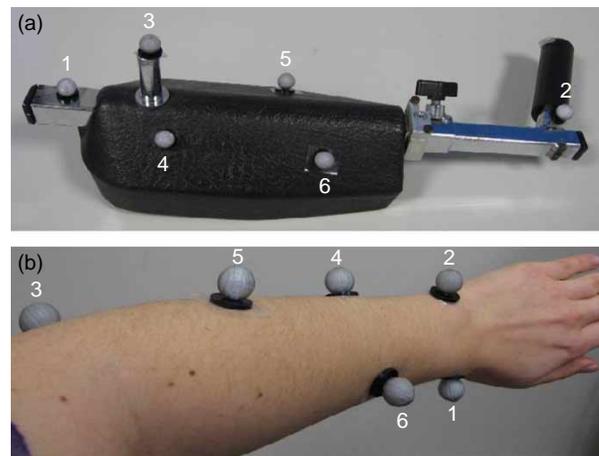

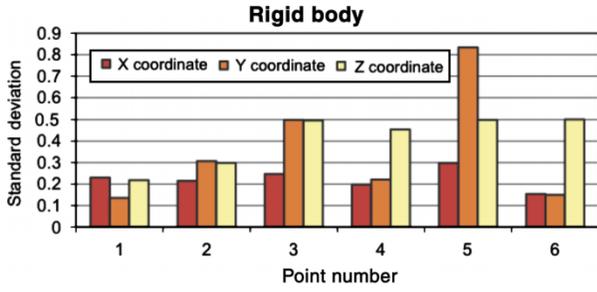Figure 1. Experiment cluster points: (a) rigid body; (b) human forearm.

Figure 2. Standard deviation of the position of each marker attached to the rigid body in the local coordinate system in three directions: (red) *x*-coordinate, (orange) *y*-coordinate, (yellow) *z*-coordinate.
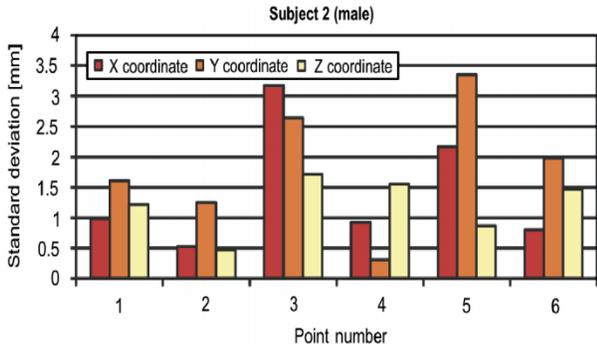

Figure 3. Standard deviation of the position of each marker attached to the human forearm in the local coordinate system in three directions: (red) *x*-coordinate, (orange) *y*-coordinate, (yellow) *z*-coordinate.

While observing these figures, one can see that the standard deviation for all points is less than 1 mm and for the majority of points is less than 0.5 mm. Also, there is no significant difference between the points. The behaviour is the same for all cluster markers.

3.2 Motion estimation based on PCT

Next we evaluated the contribution of the PCT algorithm (Fioretti and Jetto 1989; Andriacchi et al. 1998) (which meant assigning a different mass weighting factor to the cluster markers) in the reduction of the movement of the markers in the local coordinate system relative to zero state. The norm of the difference between the position at *t* and at zero state in the local coordinate system was defined as

$$\|\Delta L\|_2 = \left(\sum (|L(t) - L(0)|)^2 \right)^{1/2}. \quad (3)$$

For all points, post optimisation $\|\Delta L\|_2$ was decreased significantly. An example is given in Figure 4. As expected, the marker that was most influenced by the soft tissue deformation (marker 3) was assigned the lowest weighting factor relative to the other points (Table 1).
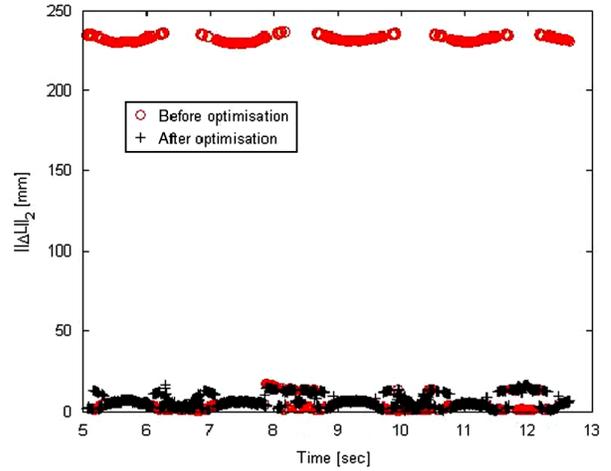

Figure 4. An example of the norm of the difference between the position at *t* and at zero state in local coordinate system of each point: (circle symbol) before optimisation and (plus sign) after optimisation.

Table 1. Second setup (human forearm motion), average weighting factor of each marker.

# Marker	1	2	3	4	4	6
Average weighting factor	0.995	1.0773	0.8874	1.3151	1.1341	1.1878
Standard deviation	0.143	0.1225	0.1824	0.2695	0.5159	0.1619

3.3 Motion estimation based on Kalman filter followed by PCT

The Kalman filter parameters were identified based on a power spectral density plot of the marker position. The 'cut-off' frequency and the spectrum upper bound were defined as $\bar{\omega} = 5$, $M = 80\,dB = 10^4$ (David 1930).

The position of the markers in the local coordinate system was calculated and compared to the calculated position in Section 3.2 (Figure 5).

Note that the movement of the markers in the local coordinate system when adding a Kalman filter is slightly reduced (Figures 5(a),(b)).

4. Experiment analysis of controlled human hand motion

4.1 Experimental setup

To evaluate the accuracy of the proposed method on human movement, a special rigid arm handle was designed (Figure 6). The handle is composed of two adjustable parts ('upper arm' and 'forearm') to allow good suitability for each tested subject and a grasping handle. The 'upper arm' is mounted on a fixed base via a shaft and a bearing. The shaft is free to rotate and is connected to a potentiometer via a coupler. This device allows a reasonably accurate
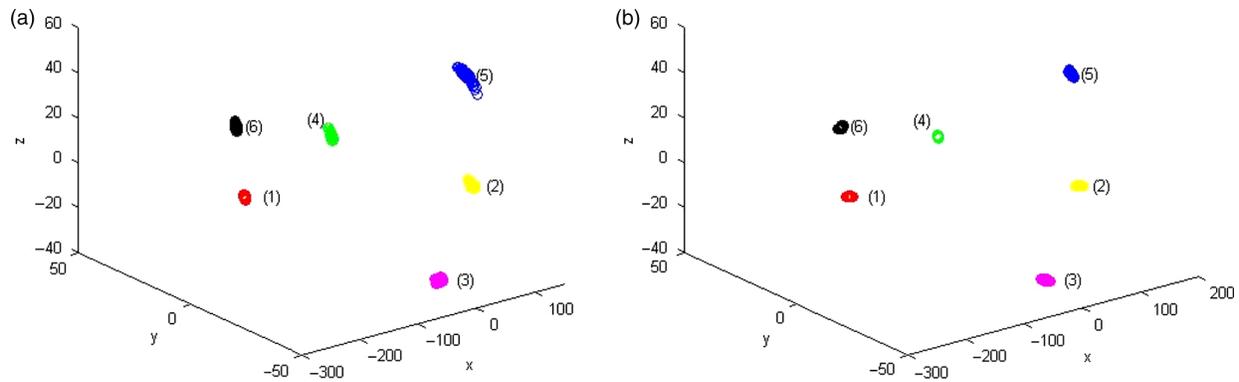
Figure 5. The position of the markers in 3D local coordinate system: (a) without the addition of Kalman filter and (b) with the addition of Kalman filter.

evaluation of the proposed method, because the subject is performing a simple planar motion and the real motion can be measured by the potentiometer readings which are equivalent to the rigid arm motion. During experiments, subjects were connected to the mechanical upper arm with two bands to prevent relative motion. The angular velocity during all experiments was similar.

In the second setup, using the human hand, the standard deviation is much bigger than in the case of the rigid body and, in most cases, greater than 1 mm.

It was also noted that there was a variation between the markers.

The potentiometer calibration (conversion of voltage to radians) was done using an optoelectronic motion capture system (Vicon). The potentiometer measured angle was filtered using a second-order low-pass digital filter (see Appendix).

Eighteen subjects participated in the experiment (Table 2):

- 10 males (25.5 ± 5 years old) with a mean BMI (weight/(height)^2) of 25.6 ± 2.9 and mean fat percentages (based on bioelectrical impedance analysis) of 21 ± 6.4% – both variables indicate normal but slightly overweight subjects.

- 8 females (24.9 ± 3 years old) with a mean BMI of (23 ± 1.5 [kg/m^2]) and mean fat percentages of 34.8 ± 3.5%. The BMI indicates a normal body mass, and the fat percentages are a bit high, but it is well known that women have higher fat percentages than men (Gallagher et al. 2000).

Each subject was asked to move the designed handle several times while his left arm was attached to it. During motion, the positions of the four markers attached to the subject's arm were measured using the motion capture system (Vicon). The markers were attached to each subject with the same orientation. The position data of the markers were synchronised with the data of the potentiometer which was also sampled by the Vicon system using the analogue interface of the Vicon system (Figure 7).

The angular motion of the system was estimated using three methods: point cluster technique (PCT), Kalman filter followed by PCT and low-pass filter followed by PCT.

Table 2. List of subject parameters for participants in the experiment.

| Subject	M/F	Age	Height [m]	Weight [kg]	BMI	Body Fat %
1	M	27	1.69	66	23.11	15
2	M	22	1.72	74.5	25.18	19.9
3	M	21	1.89	105.5	29.53	27.7
4	M	20	1.75	73	23.84	14
5	M	20	1.91	93.5	25.63	21.6
6	M	26	1.74	92	30.39	32.6
7	M	36	1.755	63.5	20.62	12
8	M	26	1.75	77	25.14	19.7
9	M	29	1.78	83.5	26.35	25
10	M	28	1.73	79	26.40	23
11	F	23	1.56	61	25.07	39.3
12	F	21	1.805	79	23.11	36.7
13	F	26	1.58	57	22.83	32.5
14	F	25	1.52	56	24.24	33.2
15	F	28	1.57	54.5	22.11	36
16	F	29	1.71	61	20.86	36
17	F	21	1.58	57	22.83	37
18	F	26	1.67	60	21.51	28
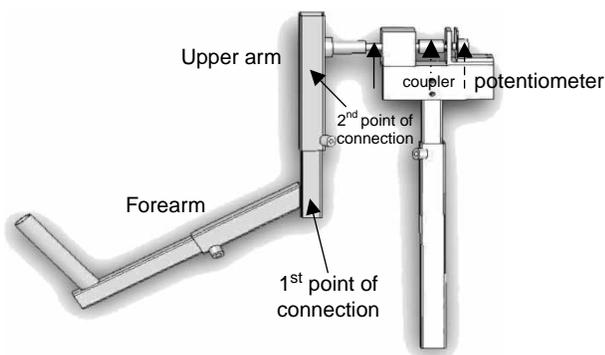
Figure 6. Designed arm handle.
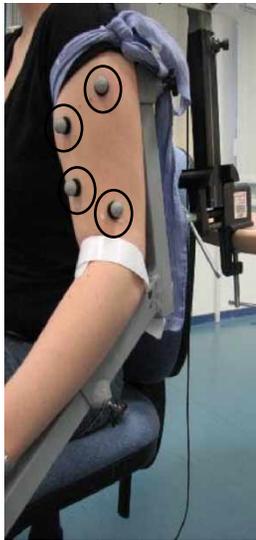
Figure 7. Human hand motion analysis, experimental setup.

The angular motion resulting from each method was then compared to the measured angle obtained by the potentiometer (ground truth).

The Kalman filter parameters were identified based on a power spectral density plot of the measured marker position (Figure 8). The cut-off frequency and the spectrum upper bound were defined as $\bar{\omega} = 5$, $M = 80\,dB = 10^4$ (Fioretti and Jetto 1989). The standard digital low-pass filter (Butterworth) cut-off frequency of $\omega = 3.5\,\text{Hz}$ was evaluated using residual analysis David (1930) (Figure 9). However, to obtain enough noise reduction and less signal distortion, the cut-off frequency was set as $\bar{\omega}_k = 5\,\text{Hz}$.

4.2 Results

Figure 10 shows an example of the potentiometer ('real'), estimated angle based on PCT, estimated angle based
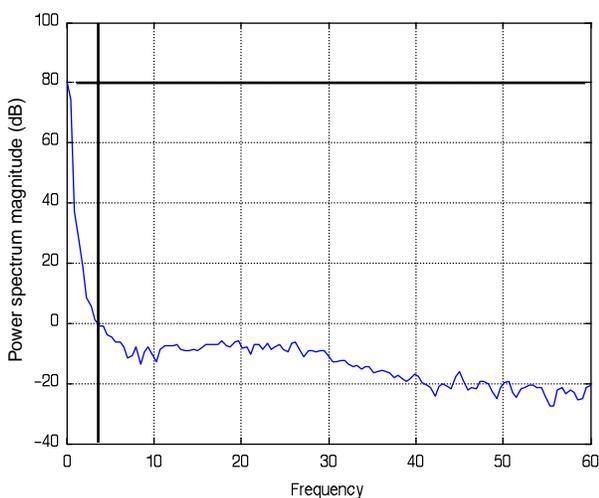

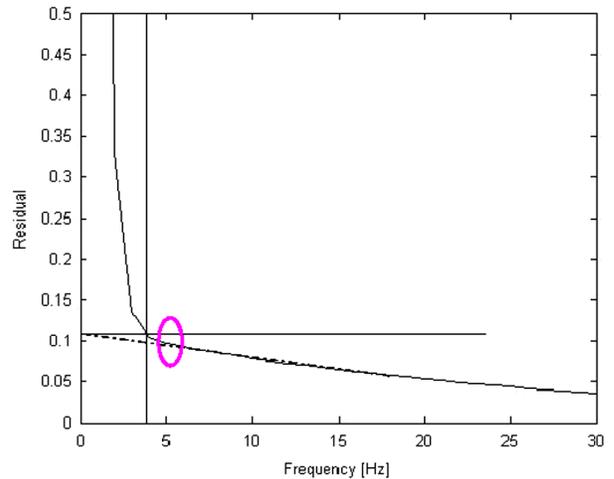Figure 8. Representative power spectral density of the data.

Figure 9. Plot of the residual between filtered and unfiltered signals as a function of the filter cut-off frequency.

on Kalman filter followed by PCT and estimated angle based on low-pass filter followed by PCT. A variable representing the accuracy of the method was defined as an integral over the absolute error:

$$I = \int |\theta_{\text{real}} - \theta_{\text{estimated}}|\,\mathrm{d}t. \tag{4}$$

The integral was computed numerically using a Matlab toolbox function ('trapz'). The accuracy evaluation of the three estimation methods is summarised in Table 3.

To validate our results, three two-sided paired *t*-tests were conducted. The first was between the error integrals of the estimated angle based on the Kalman filter followed
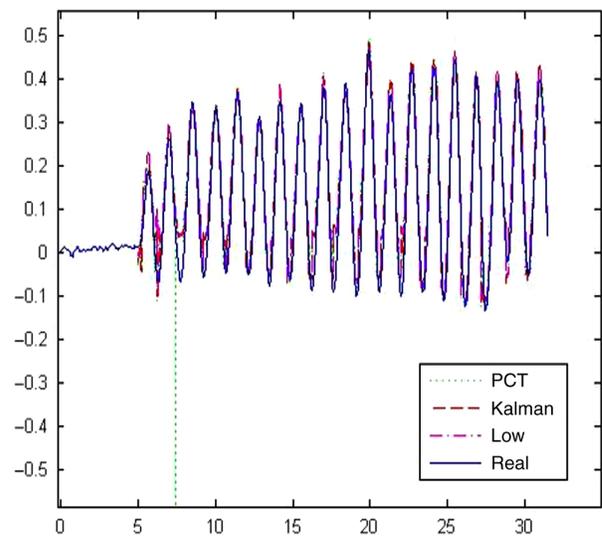

Figure 10. Example of the potentiometer ('real'), estimated angle based on PCT, estimated angle based on Kalman filter followed by PCT and estimated angle based on low-pass filter followed by PCT (subject number 1).

Table 3.   Result of the accuracy evaluation.

Subject	I (PCT)	I (Kalman filter followed by PCT)	I (Low-pass filter followed by PCT)
1	0.8294	0.8021	0.8236
2	1.8559	1.7977	1.7356
3	1.7674	1.6672	1.6746
4	0.906	0.8442	0.8314
5	1.7039	1.6446	1.5737
6	1.2545	1.2542	1.2551
7	1.6374	1.4437	1.0658
8	0.7935	0.7706	0.7458
9	0.8494	0.8343	0.7674
10	2.8433	2.8361	2.8523
11	0.4965	0.472	0.5143
12	1.2752	1.2754	1.2712
13	2.1136	2.1044	2.1232
14	4.1294	4.0585	3.9937
15	2.1724	2.1626	2.1674
16	1.3856	1.3431	1.3978
17	0.5489	0.5187	0.6
18	1.0296	0.9546	0.9166
Average	1.5329	1.488	1.4616
Standard deviation	0.899	0.895	0.8875

by PCT and the error integrals of the estimated angle based on PCT only. The test P value was 0.00085, which is statistically significant ($P < 0.01$). The intensity of the test is 80%. Therefore, it can be concluded that the two relative error integrals have different mean values. The statistical parameter d was defined as $d = I_{\text{Kalman and PCT}} - I_{\text{PCT}}$ and the calculated t parameter was (-4.0425) which is much smaller than the lower 99% confidence boundary for this case (-0.0734), meaning that the mean error integral of the estimated angle based on the Kalman filter followed by PCT is significantly smaller than the mean error integral of the estimated angle based on PCT only.
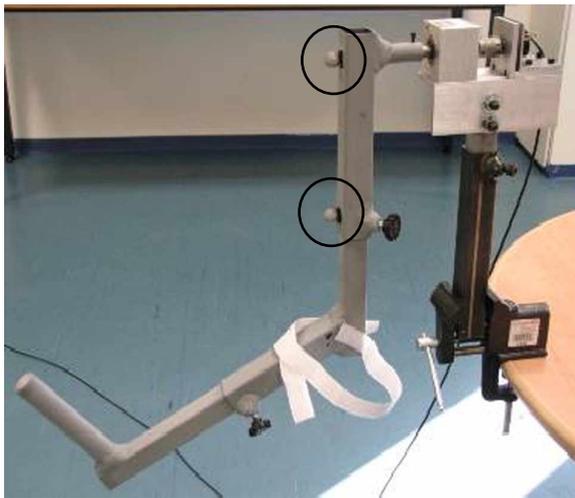

Figure 11.   Experimental setup: rigid harm handle with two markers attached to the 'upper arm'.
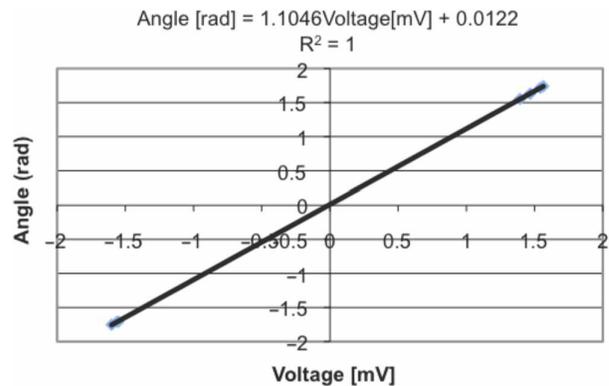

Angle [rad] = 1.1046Voltage[mV] + 0.0122, $R^2 = 1$

Figure 12.   Calibration function – linear regression.

The second paired t-test was conducted between the error integrals of the estimated angle based on the low-pass filter followed by PCT and the error integrals of the estimated angle based on PCT only. The test P value was 0.04294, which is statistically significant ($P < 0.05$). The intensity of the test is 80%. Therefore, it can be concluded that the two relative error integrals have different mean values. The statistical parameter d was defined as $d = I_{\text{low pass and PCT}} - I_{\text{PCT}}$ and the calculated t parameter was (-2.1879) which is much smaller than the lower 95% confidence boundary for this case (-0.140), meaning that the mean error integral of the estimated angle based on the low-pass filter followed by PCT was significantly smaller than the mean error integral of the estimated angle based on PCT only.

The third paired t-test was conducted between the error integrals of the estimated angle based on the Kalman filter followed by PCT and the error integrals of the estimated angle based on the low-pass filter followed by PCT. The test P-value was 0.26871, which is not statistically significant ($P > 0.05$). This means that the two groups have the same mean value and one cannot conclude that one is better than the other.

It should also be pointed out that we did not notice any correlation between BMI and fat percentages and values of the error integral. However, all subjects were young and not overweight.

5.   Discussion and closing remarks

In this work, we discussed the problem of soft tissue deformation during 3D motion analysis and its influence on the measurements and reconstruction accuracy of joint motion. Stereo-photogrammetry is widely used during 3D motion analysis. It allows for the reconstruction of joint kinematics and kinetics (i.e. forces and torques) based on the reconstruction of trajectories of markers attached to the skin surface of the body segment that is being analysed. Any relative non-rigid motion between the bony segment and the markers attached to the skin

surface introduces errors in joint kinematics and kinetics calculations. The goal is to minimise the effect of skin deformation on the resulting joint kinematics and kinetics. To confront this issue we used a combination of several existing tools: PCT and a Kalman filter.

Adding the Kalman filter to the PCT when analysing data obtained during controlled human movement trials produced a more accurate signal than the one obtained by the PCT only. However, we could not conclude that the proposed Kalman filter is better than a low-pass filter when added to the PCT. We relate this to the fact that, for the Kalman filter, we used a numerical model that does not consider any mechanical properties of the motion. We believe that the result given by the Kalman filter followed by PCT can be improved with a better modelling of the motion.

Acknowledgements

References

Alexander EJ, Andriacchi TP. 2001. Correcting for deformation in skin-based marker systems. J Biomech. 34(3):355–361.

Alexander EJ, Bergler C, Andriachhi TP. 2003. Non-rigid modeling of body segment for improved skeletal motion estimation. Comput Model Eng Sci. 4:351–364.

Anand RV, Krishna CG. 2004. Estimation of object kinematics from point data. J Mech Des. 126:16–21.

Andriacchi TP, Alexander EJ, Toney MK, Dyrby C, Sum J. 1998. A point cluster method for *in vivo* motion analysis: applied to a study of knee kinematics. J Biomech Eng. 120:743–749.

Ball KA, Pierrynowski MR. 1998. Modeling of the pliant surfaces of the thigh and leg during gait. SPIE Proc Ser. 3254:435–446.

Camomilla V, Donati M, Stagni R, Cappozzo A. 2009. Non-invasive assessment of superficial soft tissue local displacements during movement: a feasibility study. J Biomech. 42(7):931–937.

Cappello A, Cappozzo A, Lucchetti L, La Palombara PF, Leardini A. 1997. Multiple anatomical landmark calibration for optimal bone pose estimation. Hum Mov Sci. 16:259–274.

Cappello A, Stagni R, Fantozzi S, Leardini A. 2005. Soft tissue artifact compensation in knee kinematics by double anatomical landmark calibration: performance of a novel method during selected motor tasks. IEEE Trans Biomed Eng. 52(6):992–998.

Cerveri P, Rabuffetti M, Pedotti V, Ferrigno G. 2003. Real-time human motion estimation using biomechanical models and non-linear state-space filters. Med Biol Eng Comput. 41:109–123.

Cerveri P, Pedotti A, Ferrigno G. 2004. Non-invasive approach towards the *in vivo* estimation of 3D inter-vertebral movements: methods and preliminary results. Med Eng Phys. 26:841–853.

Challis JH. 1995. An examination of procedures for determining body segment attitude and position from noisy biomechanical data. Med Eng Phys. 17(2):83–90.

Che'ze L, Fregly BJ, Dimnet J. 1995. A solidification procedure to facilitate kinematic analysis based on video system data. J Biomech. 28:879–884.

Choset H, Lynch KM, Hutchinson S, Kantor G, Burgard W, Kavraki LE, Thrun S. 2005. Kalman filtering. In: Principles of robot motion: theory, algorithms, and implementation. Massachusetts Institute of Technology. p. 269–301.

David AW. 1930. Biomechanics and motor control of human movement. Ontario: Wiley. p. 33–45.

Fioretti S, Jetto L. 1989. Accurate derivative estimation from noisy data: a state-space approach. Int J Syst Sci. 20(1):33–53.

Fuller J, Liu L-J, Murphy MC, Mann RW. 1997. A comparison of lower-extremity skeletal kinematics measured using skin- and pin-mounted markers. Hum Mov Sci. 16:219–242.

Gallagher D, Heymsfield SB, Heo M, Jebb SA, Murgatroyd PR, Yoichi Sakamoto Y. 2000. Healthy percentage body fat ranges: an approach for developing guidelines based on body mass index. Am J Clin Nutr. 72(3):694–697.

Goldstein H. 1980. Classical mechanics. Reading, MA: Addison-Wesley.

Lafortune MA, Lake MJ. 1991. Errors in 3D analysis of human movement. International Symposium on 3-D Analysis of Human Movement; Montreal.

Leardini A, Chiari L, Croce UD, Cappozzo A. 2005. Human movement analysis using stereophotogrammetry part 3. Soft tissue artifact assessment and compensation. Gait Posture. 21:212–225.

Lu T-W, O'Connor JJ. 1999. Bone position estimation from skin marker co-ordinates using global optimisation with joint constraints. J Biomech. 32:129–134.

Macleod A, Morris JRW. 1987. Investigation of inherent experimental noise in kinematic experiments using super-ficial markers. In: Biomechanics X-B. Chicago, IL: Human Kinetics, Inc. p. 1035–1039.

Manal K, McClay I, Galinat B, Stanhope S. 2003. The accuracy of estimating proximal tibial translation during natural cadence walking: one vs. skin mounted targets. Clin Biomech. 18:123–131.

Reinschmidt C, Van Den Bogert AJ, Lundberg A, Nigg BM, Murphy N. 1997. Effect of skin movement on the analysis of skeletal knee joint motion during running. J Biomech. 30(7):729–732.

Ryu T, Choi HS, Chung MK. 2009. Soft tissue artifact compensation using displacement dependency between anatomical landmarks and skin markers: a preliminary study. Int J Ind Ergon. 39(1):152–158.

Soderkvist I, Wedin PA. 1993. Determining the movements of the skeleton using well-configured markers. J Biomech. 26(12):1473–1477.

Spoor CW, Veldpaus FE. 1980. Rigid body motion calculated from spatial co-ordinates of markers. J Biomech. 13(4):391–393.

Veldpaus FE, Woltring HJ, Dortmans LJ. 1988. A least-squares algorithm for the equiform transformation from spatial marker co-ordinates. J Biomech. 21(1):45–54.

Vicon Motion Systems and Peak Performance Inc. 2007. http://www.vicon.com.

Wolf A, Mor M. 2008. Rigid-body motion estimation using statistical solid dynamics method. Proceedings of the ASME Engineering Systems Design and Analysis Conference (ESDA 2008); July 7–9 2008; Haifa, Israel.

Appendix

Potentiometer calibration experiment

The potentiometer calibration (conversion of voltage to radians) was done using an optoelectronic motion capture system (Vicon). Two markers were attached to the rigid arm handle and their position in space was measured using the motion system (Figure 11).

The arm handle angle was then calculated based on the position of the two markers that were rigidly attached to the upper arm, measured using the Vicon system.

Two voltages were measured: the battery voltage (to ensure constant source voltage during the entire experiment) and the variable potentiometer voltage. The measured voltages were synchronised with the markers' trajectory measurements.

The variable potentiometer voltage is normalised by

$$V = \frac{V(t_i) - V(t_0)}{V_{\text{battery}}}, \qquad (5)$$

where $V(t_i)$ is the measured voltage at time t_i and $V(t_0)$ is the measured voltage at zero state (t_0).

Seven extremum points were compared to define a calibration function that converts the measured voltage into angle units – radians.

A linear function was fitted using the linear regression method (Figure 12):

$$\theta[\text{rad}] = 1.1046 \ \text{Voltage}[mV] + 0.0122, \qquad (6)$$

where the R-squared was found to be 1, which is an indication of a good fit.

The potentiometer signal was filtered using a second-order low-pass digital filter (Butterworth) to reduce electrical measurement noise (using Matlab). The cut-off frequency was chosen to be 7 Hz based on a residual analysis Ball and Pierrynowski (1998). The filtered and unfiltered potentiometer angles measured in an extra experiment were compared to verify that no information was lost.